Flow shaping using three-dimensional microscale gas discharge

Chin-Cheng Wang and Subrata Roy[a)]
Department of Mechanical and Aerospace Engineering, Computational Plasma Dynamics Laboratory and Test Facility, University of Florida, Gainesville, Florida 32611-6300, USA

(Received 25 May 2009; accepted 11 August 2009; published online 28 August 2009)

We introduce a flow shaping mechanism using surface compliant microscale gas discharge. A three-dimensional finite element-based multiscale ionized gas flow code is utilized to analyze charge separation, potential distribution, and flow inducement mechanism. For the case of quiescent flow, a horseshoe-shaped plasma generator is introduced. Due to its unusual shape, the three-dimensional electric force excites a pinching effect on the fluid inside selectively powered electrode arc. Such effect is capable of tripping the flow-ejecting fluid normal to the plane of the actuator and thus can be very useful for many applications. © *2009 American Institute of Physics*.
[DOI: 10.1063/1.3216046]

In recent literature, two-dimensional traditional macroscale dielectric barrier discharge (DBD) has been extensively investigated both numerically and experimentally for flow control.[1–5] However, the primary limitation of the macroscale DBD is relatively small force density (mN/cm^3) which is effective only at low flow speeds (~20 m/s). On the contrary, we have found that the microscale plasma discharge may induce force density (N/cm^3) that is order of magnitude higher.[6]

Several studies have been reported in the literature regarding discharge in microscale gap (1–100 μm).[7,8] The motivation for these are lower breakdown voltages and consequently lower power consumption in driving the discharge. Although microscale discharge has been studied experimentally for more than a decade, our understanding of the fundamental physics is still limited due to the reduced dimension, complicated transient behavior, and rapid collision in few microgaps. Numerical simulation helps circumvent these experimental challenges.

We showed in our recent study[9] that the bulk flow can be modified by actively diverting the direction of injected momentum using macroscale horseshoe plasma actuator. Appropriate polarization of such plasma generators can change flow direction from surface-parallel to surface-normal and thus may help flow turbulization. However, the mechanism for such vectored momentum injection has not been explored in microscale. Figure 1(a) describes a microscale horseshoe actuator schematic. The top view shows horseshoe-shaped inner (grounded) and outer (powered) electrodes. When the outer electrode is powered and the inner electrode is grounded, the discharge is primarily inward. The electric force from all three planar directions push fluid toward the central region, where following continuity and momentum conservation the incoming flow changes direction normal to the plane of the actuator. The electric force field in such an actuator is purely three-dimensional because of the geometry pinching the fluid at the center. This letter explores the physics of three-dimensional direct current microscale plasma discharge due to a surface compliant horseshoe shaped plasma generator and resulting momentum injection mechanism for active control of quiescent flow.

A full three-dimensional microscale plasma model, based on the two species hydrodynamic model,[1–3] is used to calculate charge density q, electric field E, potential distribution ϕ, and surrounding flow dynamics. The charge species of positive ion n_i and electron n_e, i.e., $\beta=i$, e, are derived from first principles in the form of conservation of species continuity $\partial n_\beta/\partial t+\partial n_\beta V_{\beta j}/\partial x_j=\alpha|\Gamma_e|-rn_in_e$, where $\alpha=Ap\exp[-B/(|E|/p)]$ is Townsend coefficient, and the working gas is nitrogen at bulk pressure $p=5$ Torr and temperature $T=300$ K. $|\Gamma_e|=\sqrt{(n_eV_e)_x^2+(n_eV_e)_y^2+(n_eV_e)_z^2}$ is the electron flux, and $r\sim 2\times 10^{-7}$ cm^3/s is the electron-ion recombination rate. The charge momentum uses the drift-diffusion approximation to predict general characteristics of plasma discharges. $n_\beta V_{\beta j}=\mathrm{sgn}(e)n_\beta\mu_\beta E_j-D_\beta\partial n_\beta/\partial x_j$, where μ_β is species mobility, D_β is species diffusion coefficient calculated from Einstein relation, and $E_j=-\partial\phi/\partial x_j$ is the gradient of electric potential for $1\leq j\leq 3$.

The ion mobility and diffusion at 300 K as well as electron mobility and diffusion at 11 600 K are given by Surzhikov and Shang.[10] The relation between electric potential and charge separation is given by the Poisson equation $\partial/\partial x_j(\varepsilon\partial\phi/\partial x_j)=-eq$, where e is elementary charge, $q=n_i-n_e$ is charge separation, and ε is dielectric constant. Above equations are normalized with reference time $t_0=10^{-8}$ s and reference density $n_0=10^{15}$ m^{-3}.

The averaged nitrogen velocity is governed by the continuity equation $\partial V_{nj}/\partial x_j=0$, where subscript n denote the

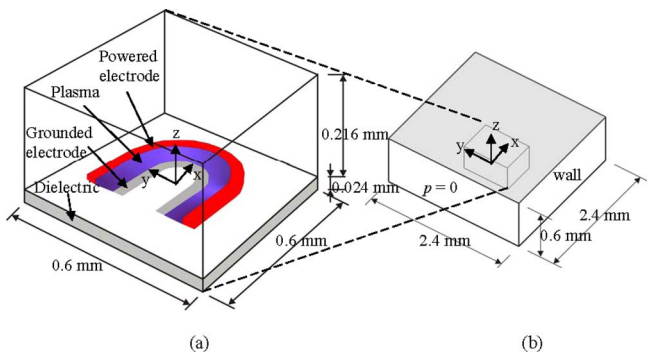

FIG. 1. (Color online) Schematic of horseshoe actuator for (a) plasma computational domain of $0.6\times 0.6\times 0.24$ mm^3 and (b) quiescent flow simulation domain of $2.4\times 2.4\times 0.6$ mm^3 showing plasma domain inlay.

a)Electronic mail: roy@ufl.edu.

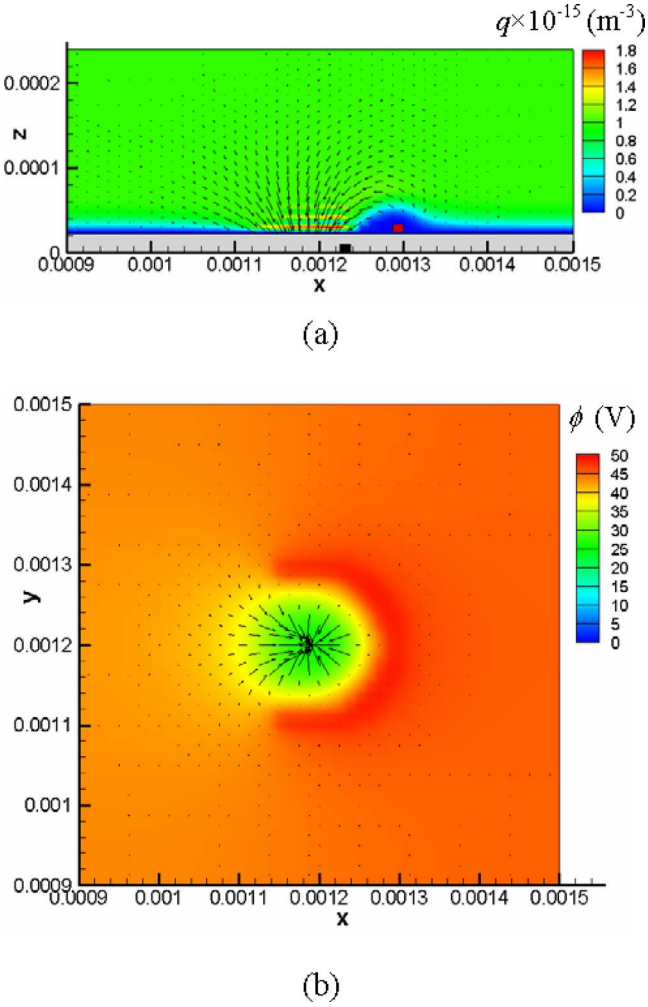

FIG. 2. (Color online) (a) Charge separation contour $q=n_i-n_e$ at x-z plane ($y=1.2$ mm) and (b) potential ϕ at x-y plane ($z=0.03$ mm) with force vectors.

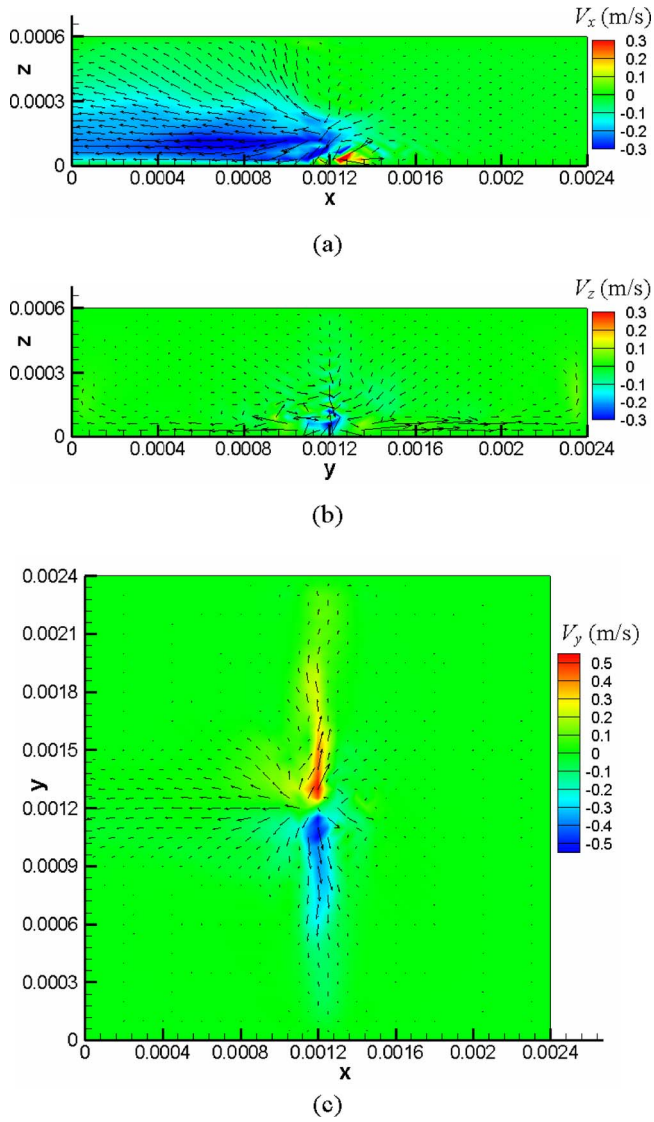

FIG. 3. (Color online) (a) V_x-velocity contour at x-z plane ($y=1.2$ mm), and (b) V_z-velocity contour at y-z plane ($x=1.2$ mm) (a) V_y-velocity contour at x-y plane ($z=0.03$ mm) with force vectors.

nitrogen gas. Due to several orders of magnitude difference in timescales of plasma and gas flow, we employ the time average of electric body force $\rho F_j=eqE_j$ in the Navier–Stokes equation $\rho DV_{nj}/Dt=\rho F_j-\nabla p+\mu\nabla^2 V_{nj}$, where ρ is the density of fluid and μ is the viscosity of fluid. For conditions stated in this letter, the Knudsen number (Kn) is less than 0.008 validating the use of no-slip condition.[11]

Both hydrodynamic plasma model and Navier–Stokes equations are solved by the finite element based multiscale ionized gas (MIG) flow code. MIG flow code has been utilized for a range of applications including microscale flows and plasma physics.[1–3,6,11] A fully implicit time stepping procedure along with the Newton–Raphson scheme is used for dealing with this nonlinear problem. For solving a sparse resultant stiff matrix, an efficient generalized minimal residual solver is utilized to calculate the charge separation, electric field, and fluid velocity. The solution of the Newton iteration is considered convergent when the L_2 norms of all the normalized solution variables and residuals drop below a convergence criterion of 10^{-3}.

The lower part of the computational domain consists of a 0.024-mm-thick dielectric with zero charge density while the upper part consists of a fluid domain ($0.6\times0.6\times0.216$ mm^3) filled with nitrogen gas shown in Fig. 1(a). The exposed (red) electrode of the horseshoe actuator is at the center of the domain on the dielectric surface at $z=0.024$ mm while the embedded electrode is grounded at $z=0$. A direct current voltage of $\phi=50$ V is applied to the exposed electrode. Note that the electrodes are shown here as references and they have negligible thickness. Figure 1(b) shows the computational domain ($2.4\times2.4\times0.6$ mm^3) for quiescent flow simulation and the inner domain which is at the center of the outer domain for plasma simulation. We assume zero pressure for both boundaries at x-direction and all other boundaries with no-slip wall condition. The computational domain was discretized using $48\times48\times40$ three-dimensional trilinear elements with 98 441 nodes sufficient to capture the sheath (Debye length) physics for plasma simulation. The fluid physics is resolved with a mesh of $48\times48\times20$ three-dimensional trilinear elements overlaid on top of the plasma mesh.

Figure 2 shows the electric force vector distribution overlay on (a) charge separation $q=n_i-n_e$ at x-z plane ($y=1.2$ mm) and (b) potential distribution at x-y plane ($z=0.03$ mm). We can see that the potential ϕ varies from 50 to 0 V calculated from Poisson equation. The force density

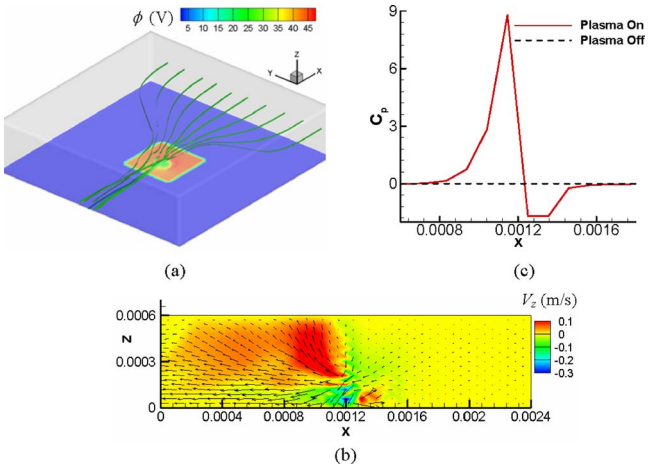

FIG. 4. (Color online) (a) Green fluid lines with potential (ϕ) contour at bottom for quiescent flow, (b) V_z-velocity contour at x-z plane ($y=1.2$ mm) with force vectors, and (c) pressure coefficient along (x, 1.2, 0.03 mm).

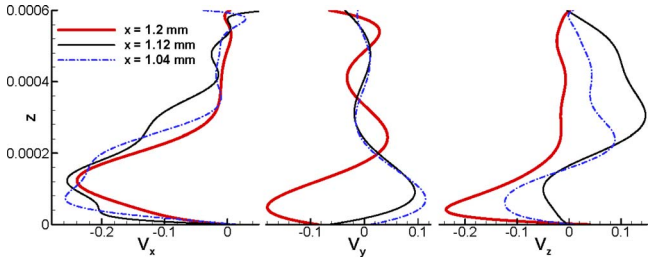

FIG. 5. (Color online) Induced velocity components along the z-direction at three x locations for $y=1.2$ mm.

for this electrode arrangement (not shown) is on the order of kN/m^3. The quasisteady state solution for the peak of separated charge is close to the dielectric surface inside the exposed electrode of the horseshoe actuator. The peak charge density is about 10^{15} m^{-3}. In the top view, just above dielectric surface at $z=0.03$ mm shown in Fig. 2(b), we can easily see the distribution of the electric force vectors acting inward.

Figure 3 describes the effect of horseshoe actuator on quiescent flow in three different planes. The center of the horseshoe is located at (x, y, z: 1.2, 1.2, 0 mm). The electric force attracts fluid toward the center of the horseshoe as shown in Fig. 3(a) and pushes fluid to the left boundary. The effect of plasma force acting inward acting is to extract fluid from top of plasma region ($y=1.2$ mm) and eject it to both the boundaries shown in Fig. 3(b). This pinching effect is evident in the $z=0.03$ mm plane shown in Fig. 3(c). The fluid is separated into two halves. As a result, the working fluid is ejected outward and nearly normal to the plasma region. The fluid at the center of horseshoe actuator is almost stagnant.

Figure 4(a) plots the induced flow streamtraces (colored by green) for quiescent flow condition. The bottom wall is colored by potential (ϕ) for recognizing the location of the electrodes. We can see the electric force attracts the fluid from outside the horseshoe actuator and trips the fluid lines in the plasma regime. Such a tripping mechanism creates plasma barriers to push the flow toward the central region and ejects the fluid normal to the plane of the actuator as shown in Fig. 4(b). The pressure coefficient calculated based on the peak-induced velocity also shows a sharp rise (stagnant point) followed by a quick drop denoting rapid change in the flow direction. Corresponding plasma induced velocity components at three separate x locations are plotted in Fig. 5. While the force density for such microscale actuators is calculated to be order of kN/m^3, the control volume in which this electric force is active is orders of magnitude smaller, exerting ~ 0.1 mN/m net force on the surface and inducing a velocity of 0.1 m/s. We note that for air chemistry the electron loss will increase.[12] So, the force density in air will be higher inducing higher flow rate than in the case with nitrogen. For such microdischarge, the steady state current density near the cathode is estimated to be ~ 0.1 A/cm^2. Horseshoe discharge area is around 2.6×10^{-4} cm^2. Hence the current and real power requirements are estimated to be $\sim 2.6\times10^{-5}$ A and ~ 1.3 mW, respectively.

In conclusion, a three-dimensional plasma simulation based on first-principles method demonstrates flow shaping using a surface compliant horseshoe plasma generator. When the outer electrode is powered and the inner electrode is grounded, the electric force distribution is calculated based on the charge separation and the potential gradient. Results demonstrate that the induced electric force pinches the fluid inside the plasma generator so as to trip the flow field normal to the dielectric surface. Such low power generators may be useful for many applications that involves flow shaping, thrust vectoring, and device cooling.

[1]S. Roy, Appl. Phys. Lett. **86**, 101502 (2005).
[2]H. Kumar and S. Roy, Phys. Plasmas **12**, 093508 (2005).
[3]S. Roy and D. Gaitonde, Phys. Plasmas **13**, 023503 (2006).
[4]K. P. Singh and S. Roy, J. Appl. Phys. **103**, 013305 (2008).
[5]D. F. Opaits, G. Neretti, A. V. Likhanskii, S. Zaidi, M. N. Shneider, R. B. Miles, and S. O. Macheret, Proceedings of the 38th AIAA Plasma Dynamics and Lasers Conference, 2007 (unpublished), Paper No. AIAA-2007–4532.
[6]C. C. Wang and S. Roy, J. Appl. Phys. **106**, 013310 (2009).
[7]L. Baars-Hibbe, P. Sichler, C. Schrader, N. Lucas, K.-H. Gericke, and S. Büttgenbach, J. Phys. D: Appl. Phys. **38**, 510 (2005).
[8]E. Hourdakis, G. W. Bryant, and N. M. Zimmerman, J. Appl. Phys. **100**, 123306 (2006).
[9]S. Roy and C. C. Wang, J. Phys. D: Appl. Phys. **42**, 032004 (2009).
[10]S. T. Surzhikov and J. S. Shang, J. Comput. Phys. **199**, 437 (2004).
[11]S. Roy, R. Raju, H. F. Chuang, B. A. Cruden, and M. Meyyappan, J. Appl. Phys. **93**, 4870 (2003).
[12]K. P. Singh and S. Roy, J. Appl. Phys. **101**, 123308 (2007).